Acta Biomaterialia 43 (2016) 358–368

Contents lists available at ScienceDirect

Acta Biomaterialia

journal homepage: www.elsevier.com/locate/actabiomat

Full length article

Hypoxia-mimicking Co doped TiO_2 microporous coating on titanium with enhanced angiogenic and osteogenic activities

Jianhong Zhou [a], Lingzhou Zhao [b,*]

[a] Institute of Physics & Optoelectronics Technology, Baoji University of Arts and Sciences, Baoji 721016, China
[b] State Key Laboratory of Military Stomatology, Department of Periodontology, School of Stomatology, The Fourth Military Medical University, Xi'an 710032, China

ARTICLE INFO

Article history:
Received 19 March 2016
Received in revised form 20 July 2016
Accepted 27 July 2016
Available online 28 July 2016

Keywords:
Implant coating
Cobalt
Mesenchymal stem cell
Hypoxia-inducible factor-1a
Osseointegration

ABSTRACT

Advanced titanium (Ti) based bone implant with both angiogenesis and osteogenesis stimulating activities for enhanced clinical performance is stringently needed. In the present work, TiO_2/calcium-phosphate (TCP) coatings on Ti doped with cobalt (Co) of various amounts (designated as C2-TCP, C7-TCP, and C13-TCP where the Arabic numbers indicate the mean Co contents) are developed by a simple micro-arc oxidation procedure. The Co doped TCP coatings possess a microporous structure (pore size of 3–4 μm in average diameter) which is evenly covered by nano-grains of 30–60 nm in size. Successful Co incorporation in TCP is determined by X-ray photoelectron spectroscopy. The microstructure, TiO_2 phase compositions, surface roughness, and wettability of TCP are not apparently affected by the Co incorporation. The Co doped coatings bond firmly to the Ti substrate and show good long-term adhesion strength stability in biological environment. Then the behaviors of rat bone marrow stem cells (MSCs) on the Co-incorporated TCP are evaluated. The Co incorporation leads to enhanced expression of the markers for both angiogenesis and osteogenesis, and the effects are positively related to the incorporated Co amount. Overdose of Co incorporation (C13-TCP) can induce certain cytotoxicity and an optimal dose of Co incorporation is essential to get the enhanced angiogenic and osteogenic activities without showing cytotoxicity. Between C2-TCP and C7-TCP that show no significant cytotoxicity, C7-TCP exhibits higher angiogenic and osteogenic activities. In conclusion, the Co doping is feasible to enhance the angiogenic and osteogenic activities of orthopedic and dental Ti implants for potentially improved clinical performance.

Statement of Significance

TiO_2/calcium-phosphate coatings on Ti doped with cobalt are developed by a simple micro-arc oxidation procedure. The Co doped coatings bond firmly to the Ti substrate and show good long-term adhesion strength stability in biological environment. Furthermore, the cobalt doping is feasible to enhance the angiogenic and osteogenic activities of orthopedic and dental Ti implants for potentially improved clinical performance.

1. Introduction

Currently, titanium (Ti) based bone implants have been widely applied to treat bone fracture or defect in orthopedic clinic as well as to restore the missing teeth in dental clinic [1,2]. Though a high success rate of nearly 95% has been achieved for the Ti implants in healthy patients [3], they still display inadequate bioactivity that may result in compromised lifespan, especially when encountering some complicated conditions that do not benefit the osseointegration, such as osteoporosis. It is generally believed that mesenchymal stem cells (MSCs) play a key role in the osseointegration. Most of the osteoblastic cells that colonize the implant surface to form bone originate from MSCs [4]. Thus to accomplish good osseointegration, it is critical for an implant surface to have the osteogenic activity to promote the differentiation of MSCs preferentially towards osteoblasts in lieu of other lineages that hinder the osseointegration, such as adipocytes. Accordingly, a lot of researches are dedicated to assessing or improving the osteogenic ability of bone implants.

* Corresponding author at: State Key Laboratory of Military Stomatology, Department of Periodontology, School of Stomatology, The Fourth Military Medical University, No. 145 West Changle Road, Xi'an 710032, China.
E-mail address: zhaolingzhou1983@hotmail.com (L. Zhao).

http://dx.doi.org/10.1016/j.actbio.2016.07.045
1742-7061/

It is more and more recognized that an ideal osseointegration establishment also requires quick and good neovascularization which not only provides nutrition supply for the cell survival and proliferation but facilitates the distant homing of MSCs to the implant surface [5]. Several approaches have been proposed to enhance the angiogenic property of biomaterials, such as pre-vascularization via endothelial cell culture as well as incorporation of angiogenic growth factors including basic fibroblast growth factor, vascular endothelial growth factor (VEGF), and platelet-derived growth factor [6–10]. Nonetheless, these methods are complex and the usage of growth factors has many disadvantages including high cost, short half-life, instability, as well as the safety concern from the recombinant proteins [11], hindering their potential clinical translation.

To obtain advanced Ti implant with the desired angiogenic and osteogenic activities, loading and delivering of inorganic bioactive elements shall be a more feasible strategy. The inorganic elements are quite stable facilitating the incorporation process and the storage. Meanwhile, they generally function at very low doses, so relatively long-term activities can be expected from the Ti implant surface of so limited reservoir [12]. Cobalt (Co) is an essential trace element and acts as a cofactor of many metalloproteins in the body [13,14]. The Co ions can stabilize the hypoxia inducible factor-1a (HIF-1a) and subsequently activate the HIF-1a target genes such as VEGF, and thus have been used extensively to simulate a hypoxic environment *in vitro* [15,16]. Co incorporated mesoporous bioactive glass, β-Tricalcium phosphate ceramics, and hydroxyapatite were reported to have a hypoxia mimicking effect and show improved angiogenic property [17–21]. Unexpectedly, the Co incorporation was also reported to enhance the osteogenic activity of biomaterials by up-regulating the bone-related gene expression in MSCs [17–19]. Accordingly, the Co incorporation shall constitute an effective strategy for developing implants with both angiogenic and osteogenic activities, especially when combined with proper implant surface topographical modification. It should be noted that overdose of inorganic elements will induce toxicity [17], and hence optimizing their incorporation dose is essential.

Regarding the method for the inorganic element incorporation to the Ti implant surface, micro-arc oxidation (MAO) is a feasible choice, which has proven to be an effective means to incorporate the inorganic elements, such as calcium (Ca), phosphorus (P), strontium (Sr), and zinc (Zn) to the Ti surface [22–24]. MAO can give rise to a firmly adherent microporous TiO_2 coating on the Ti surface [25], which has been widely investigated to show enhanced bioactivity [22–25] and some MAO modified implants have long been used in clinic. In the present study, TiO_2/Ca-P microporous (TCP) coatings incorporated with different amounts of Co, namely C2-TCP, C7-TCP, and C13-TCP, where the Arabic numbers indicate the mean Co contents in the coatings, were developed by the MAO process on Ti. *In vitro* MSC culture model was used to investigate whether they possess favorable cytocompatibility and angiogenesis and osteogenesis enhancing effects.

2. Materials and methods

2.1. MAO treatment of pure Ti

A bipolar pulse power supply was employed for the MAO treatment of Ti disks. The pure Ti disks (size of $\phi 15 \times 2$ mm) were used as anodes and treated in distilled water electrolytes containing different concentrations of calcium acetate (CaA), cobalt acetate (CoA), and β-glycerophosphate disodium (β-GP) (Table 1) with an applied positive pulse voltage of 410 V, a negative pulse voltage of 100 V, a pulse frequency of 100 Hz, and a duty ratio of 26% for 5 min. During the MAO treatment, the electrolyte was cooled with water of 4 °C. The MAO treated Ti samples were ultrasonically washed with alcohol and distilled water, and then dried at room temperature.

2.2. Surface characterization

The morphology and elemental compositions of the coatings were examined by a field emission scanning electron microscope (FESEM; JEOL JSM-6700F, Japan) equipped with an energy-dispersive X-ray spectrometer (EDX) operating at 20 kV. Phase identification was carried out with thin film X-ray diffraction (TF-XRD) (D/max-RB, Rigaku, Japan) using a Cu Kα irradiation in the regular range of $2\theta = 20–70°$ with an accelerating voltage of 40 kV, a current of 100 mA and a scanning speed of 4°/min. The elements and chemical species of the coatings were examined with X-ray photoelectron spectroscopy (XPS; Axis Ultra, UK) under the conditions of working voltage 2 kV, current 2 μA, oblique angle 45° and spot diameter 500 μm. In the XPS test, monochromatic Mg Kα radiation was used as an X-ray source, and the photoelectron take-off angle was set at 45°. The obtained XPS spectra were calibrated to the C1s (hydrocarbon C—C, C—H) contribution at the binding energy of 284.8 eV. The roughness of the coatings was examined by atomic force microscopy (AFM; SPM-9500J3, Japan) in tapping mode with a scan rate of 1 Hz and a scan size of 40 μm × 40 μm, using a Si_3N_4 cantilever with a spring constant of 0.12 N/m (Seiko Instruments) for resolution imaging. The hydrophilicity of the coatings was measured by a surface contact angle measurement machine (DSA30, Kruss, Germany).

2.3. Ion release and adhesion strength of the coatings to the substrate

The specimens were immersed in 10 mL α-minimum essential medium (α-MEM) (Life Technologies, USA) at 37 °C for 0, 1, 3, 6, 14, and 28 days, successively. At the pre-determined time points, the leaching liquid was collected and the concentrations of Ca, P, and Co ions released were measured by inductively coupled plasma-mass spectrometry (ICP-MS; Nu Instruments, Wrexham, UK). Meanwhile, the Ca, P, and Co ions concentrations in fresh α-MEM were measured as the background using the above-mentioned method. The difference of the ion concentrations between the specimen-immersed α-MEM and the fresh α-MEM

Table 1
The corresponding MAO electrolyte compositions and the elemental compositions of the coatings surfaces detected by XPS.

Coatings	Aqueous electrolyte concentration (M)			Elemental composition (wt.%)				
	CaA	β-GP	CoA	Ti	O	Ca	P	Co
TCP	0.05	0.02	–	47.8 ± 0.7	41.3 ± 0.6	6.4 ± 0.2	4.5 ± 0.3	–
C2-TCP	0.05	0.02	0.02	44.1 ± 0.9	43.7 ± 0.5	5.8 ± 0.6	4.3 ± 0.2	2.1 ± 0.1
C7-TCP	0.05	0.02	0.06	43.4 ± 1.1	38.6 ± 0.4	6.2 ± 0.5	4.6 ± 0.4	7.2 ± 0.2
C13-TCP	0.05	0.02	0.10	40.2 ± 0.7	37.1 ± 0.9	5.9 ± 0.3	4.1 ± 0.3	12.7 ± 0.4

indicates the concentrations of ion release from the coatings. The ion release tests were performed on five replicate samples (n = 5).

At the same time, ion release of the coatings in the presence of cells was measured. One mL culture medium containing 2×10^4 MSCs was seeded on the Ti samples, and cultured at 37 °C in a humidified atmosphere of 5% CO_2 and 95% air for 0, 1, 3, and 6 days. It is worth noting that the culture medium wasn't refreshed. At the pre-determined time points, the culture medium was collected and the concentrations of Ca, P, and Co ions released were measured used the above methods. In order to compare with ion release of the coatings in the absence of cells, the concentration of ion release of the coatings in the presence of cells need ten times dilution. The ion release tests were performed on five replicate samples (n = 5).

Scratch tests of the samples after immersion in α-MEM for different durations were performed using an auto scratch coating tester to evaluate their adhesion strengths to the substrate. The critical load (Lc) was defined as the smallest load at which a recognizable failure occurred, and was determined from the load versus acoustic output characteristics. The Lc of each coating was the average of five samples.

2.4. Protein adsorption assay

For protein adsorption assay, a 1 mL droplet of α-MEM with 10% fetal bovine serum (FBS; Life Technologies, USA) was pipetted onto each sample placed in the 24-well plate. After incubation in the medium for 24 h at 37 °C, the proteins adsorbed onto the samples were detached by 1% sodium dodecyl sulfate (Solarbio) and determined with a MicroBCA protein assay kit (Pierce). Five samples for each group were tested.

2.5. MSC harvest and culture

MSCs were harvested from 1-week-old New Zealand rabbits [26]. The animal experiments were conducted according to the ISO 10993-2:1992 animal welfare requirements and approved by the Institutional Animal Care and Use Committee (IACUC) of Xi'an Jiaotong University. Briefly, the bone marrow was aspirated from the femora and tibias, from which the mononucleated cells were isolated via density gradient centrifugation. The cells obtained were plated in the cell culture flasks containing 20 mL of a-MEM containing 10% FBS and 1% antibiotics, and cultured at 37 °C in a humidified atmosphere of 5% CO_2 and 95% air. The non-adherent cells were removed and the adherent cells were collected for further expanding. All experiments were performed within passage 3. The MSC suspension of 1 mL containing 2×10^4 cells was seeded on the Ti samples.

2.6. Cytotoxicity, cell adhesion, proliferation, and morphology

The activity of lactate dehydrogenase (LDH) released by the cells in the culture media was used as an index for the cytotoxicity of the Ti samples. After culturing of the cells on the Ti samples for 3 days, the culture medium was collected (among this period the medium was not changed) and centrifuged, and the LDH activity in the supernatant was determined spectrophotometrically according to the manufacturer's instruction (Sigma, USA).

The cell counting kit-8 (CCK-8) assay was used to assess the adhesion and proliferation of MSCs after culture of 1 h, 5 h, 24 h, 3 days, 7 days, and 14 days.

The live/dead staining using the LIVE/DEAD Viability/Cytotoxicity Kit (Invitrogen, France) was performed to identify the viable and nonviable MSCs on the samples after 7 days of incubation. The samples with adherent cells were washed thrice with PBS followed by the addition of 500 μL of PBS containing ethidium-homodimer-1 (4 μM) and calcein-AM (2 μM) to each well prior to incubation at 37 °C for 30 min. The fluorescence-stained cells were analyzed using an OLYMPUS laser confocal microscope (FV1000) for the collection of images of four random fields on each sample.

After 3 days of incubation, the samples with attached MSCs were washed with PBS, fixed in 3% glutaraldehyde, dehydrated in a graded ethanol series, freeze-dried, and sputter-coated with gold prior to observation by the FESEM.

After 3 days of incubation, the cell-seeded samples were fixed with 4% paraformaldehyde and washed thrice with PBS buffer (PBS supplemented with 0.05% Tween-20; Sigma), permeabilized with 0.1% Triton X-100 (Sigma) and washed thrice again with the PBS buffer. The cells were then incubated for 30 min at room temperature in 1% bovine serum albumin (Sigma) blocking agent. Then, 37.5 ng/mL tetrameth-ylrhodamine isothiocyanate-conjugated phalloidin was added to the cells and incubated at 37 °C for 60 min for the actin staining. Subsequently, the cells were washed thrice with PBS and counterstained in 0.1 μg/mL 6-diamidino-2-phenylindole (DAPI) at 37 °C for 5 min. After washing thrice with PBS, the stained cells were analyzed with an OLYMPUS laser confocal microscopy FV1000 (Tokyo, Japan).

2.7. Quantitative real-time PCR assay

After culturing for 3, 7, and 14 days, the total RNA was isolated using the TRIzol reagent (Life Technologies, USA), and 1 μg RNA from the cells on each sample was reversed transcribed into complementary DNA using a PrimeScrip RT reagent kit (TaKaRa, Japan). The expression of key angiogenic factors (VEGF and HIF-1a) and osteogenic differentiation markers (alkaline phosphatase (ALP) and osteocalcin (OCN)) was quantified on a quantitative real-time polymerase chain reaction (qRT-PCR) detection system (Bio-Rad iQ5 Multicolor) with SYBRPremix ExTaqII (TaKaRa, Japan). Data analysis was carried out using an iQ5 Optical System (Bio-Rad, USA) with software version 2.0. The expression levels of the target genes were normalized to that of the housekeeping gene glyceraldehyde-3-phosphate dehydrogenase (GAPDH). The primers for the target genes were listed in Table 2.

2.8. Intracellular ALP activity and contents of specific proteins

After 3, 7, and 14 days of culture, the cell-seeded samples were washed thrice with PBS, lysed in 0.1vol% Triton X-100 (Life Technologies, USA) through five standard freeze-thaw cycles, and finally shaken for 10 min. The intracellular contents of proteins (VEGF, HIF-1a, and OCN) and the ALP activity in the cell lysates were determined with ELISA (Bluegene Ltd., China). The optical absorbance at 450 nm was recorded spectrophotometrically, and the ALP activity and protein contents of MSCs cultured on the samples were drawn from a standard curve of absorbance versus known standards of corresponding proteins run in parallel with the experimental samples. The results were normalized to the intracellular total protein content. Five samples for each group were tested (n = 5).

Table 2
Primers used for qRT-PCR.

Gene	Forward primer sequence (5′–3′)	Reverse primer sequence (5′–3′)
VEGF	TTGAGTTGGGAGGAGGATGT	TGGCAGGCAAACAGACTTC
HIF-1a	CGATGACACGGAAACTGAAG	CAGAGGCAGGTAATGGAGACA
ALP	CTGAGCGTCCTGTTCTGAGG	GTTCCTGGGTCCCCTTTCTG
OCN	CTTCGTGTCCAAGAGGGAGC	CAGGGGATCCGGGTAAGGA
GAPDH	ATCAAGTGGGGTGATGCTGG	TACTTCTCGTGGTTCACGCC

2.9. Collagen secretion and extracellular matrix mineralization

Collagen secretion and extracellular matrix (ECM) mineralization on the samples was assessed after 3, 7 and 14 days of culture by the Sirius Red and Alizarin Red staining, respectively. After washing with PBS and fixation, the samples were stained using 0.1% Sirius Red (Sigma, USA) to reveal the collagen secretion and 40 mM Alizarin Red (pH 4.2, Sigma, USA) to show the mineralization. In the quantitative analysis, the Sirius Red or Alizarin Red stain on the specimen after washed with 0.1 M acetic acid or distilled water was dissolved in 0.2 M NaOH/methanol (1:1) or 10% cetylpyridinium chloride (Acros) to measure the optical density at 540 or 620 nm.

2.10. Statistical analysis

The data were expressed as mean ± standard deviation (SD) from three independent experiments. The data were analyzed using SPSS 14.0 software (SPSS, USA). A one-way ANOVA followed by a Student-Newman-Keuls *post hoc* test was used to determine the level of significance. $p < 0.05$ and 0.01 was considered to be significant and highly significant, respectively.

3. Results and discussion

3.1. Characterization of the coatings

Fig. 1a shows the surface morphology of TCP, C2-TCP, C7-TCP, and C13-TCP. It can be seen that all coatings have similar typical microporous MAO structure without noticeable difference. The micropores of an average diameter of 3–4 μm distribute homogeneously. The higher magnification images further show that all the coatings are evenly covered with the nano-grains of ~30–60 nm in size (top insets in Fig. 1a). The EDX results (bottom insets in Fig. 1a) show that only Ti, O, Ca, and P are detected in TCP, while for C2-TCP, C7-TCP, and C13-TCP, Co can be further detected. Table 1 summarizes the surface elemental compositions of the coatings detected by XPS. The results show that the Co content in the coatings can be modulated by the CoA concentration in the MAO electrolytes, which show a positive correlation. The elemental distribution on the cross-section of C7-TCP (Fig. 1b) again shows that the coating contains Ca, P, and Co besides the predominant elements of Ti and O, which further confirms the successful incorporation of Co in the C7-TCP coating. There is no discontinuity

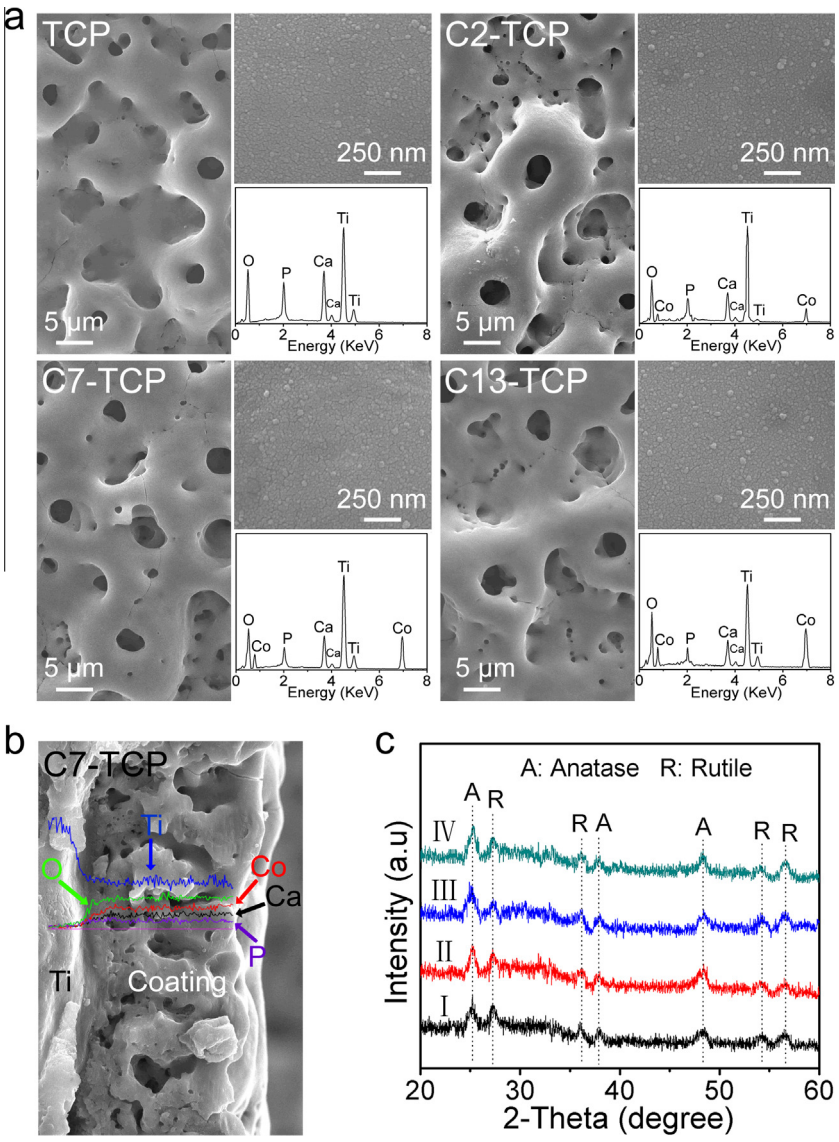

Fig. 1. (a) SEM surface morphologies of TCP, C2-TCP, C7-TiCP, and C13-TCP. The top insets show the magnified images and the bottom insets show the EDX pattern. (b) Cross-sectional image of C7-TCP and the elemental distribution, and (c) TF-XRD patterns of TCP (I), C2-TCP (II), C7-TCP (III), and C13-TCP (IV).

at the interface of the coating/Ti substrate (Fig. 1b), exhibiting a firm binding of the coating to the Ti substrate.

The TF-XRD patterns of TCP, C2-TCP, C7-TCP, and C13-TCP are shown in Fig. 1c. All coatings consist of predominant anatase and rutile TiO_2. The Co incorporation leads to slight change in the phase compositions of the coating. However, no feature peaks of Co-containing compounds are detected in any sample by TF-XRD.

The XPS full spectrum obtained from C7-TCP, as a representative of the Co incorporated coatings, is shown in Fig. 2a. Besides the feature peaks of Ti, O, Ca, and P, the feature peaks of Co are also detected, confirming the successful Co incorporation in C7-TCP. The high-resolution spectra of the coating are shown in Fig. 2b–f. The Ti2p spectrum corresponds to typical binding energies for TiO_2 [27]. The O1s spectrum is deconvoluted into two Gaussian component peaks. The peak located at 530.1 eV is assigned to O1s in TiO_2 [27,28], and the other peak at 531.3 eV corresponds to O1s in P═O— groups ($Ca_3(PO_4)_2$ or $CaHPO_4$) [29,30]. The Ca2p peaks are located at 347.1 eV and 350.7 eV, and the P2p peak is located at 133.3 eV, which indicated that the Ca2p and P2p exists in the form of calcium phosphate phases (such as α-tricalcium phosphate, amorphous calcium phosphate) in the detected surface layer [31]. The Co2p peak is located at 780.3 eV, assigned to Co2p in $CoTiO_3$ [32].

The roughness values of the coatings measured by AFM are listed in Table 3. There are no significant difference in the micro-scale roughness among the different coatings, as characterized by the average roughness (Ra), root-mean-square roughness (RMS), and selection of 10-point height of irregularity roughness (Rz). Meanwhile, the water contact angles on TCP, C2-TCP, C7-TCP, and C13-TCP are also very similar. Totally, the Co incorporation does not apparently alter the surface roughness and wettability of the MAO coating.

All the surface properties of a biomaterial including surface chemistry, surface energy/wettability, surface roughness and surface topography can influence its biological performance [33]. The different Ti coatings fabricated in this study have the same microporous feature and TiO_2 phase compositions, and the similar surface roughness and wettability. Therefore, one can assess the effects of Co incorporation of different doses and the according Co release on the biological performances of the Ti implant without considering the other influencing factors.

Table 3
Roughness values, and contact angles of the coatings.

Coatings	Roughness (nm)			Contact angle (deg.)
	Ra	RMS	Rz	
TCP	428 ± 45	462 ± 36	1193 ± 146	45.3 ± 3.5
C2-TCP	462 ± 43	474 ± 34	1234 ± 142	46.8 ± 4.1
C7-TCP	461 ± 40	481 ± 41	1215 ± 153	44.6 ± 3.8
C13-TCP	468 ± 38	483 ± 39	1224 ± 149	45.2 ± 4.6

3.2. Ion release and adhesion strength of the coatings to the substrate

Fig. 3 shows the release of ions and the adhesion strength of the coatings to the substrate after immersion in α-MEM of different durations in the absence of cells and in the presence of cells. In the absence of cells (Fig. 3a) TCP can release the Ca and P ions, and C13-TCP, C7-TCP, and C2-TCP can release the Co ion furthermore. The doses of the Co, Ca, and P ions released increase commensurate with the soaking duration, indicating a constant release mode. For the Co ion release, generally there is a controlled release profile. The released Co doses are in line with the incorporated Co amounts in the coatings, following the order of C13-TCP > C7-TCP > C2-TCP. In addition, the Co incorporation and release does not obviously influence the release profiles of Ca and P ions. Compared to the Co, Ca, and P ion release of the coatings in the absence of cells (Fig. 3b), the ion release in the presence of cells is lower probably because of the diffusional impediments from the protein adsorption, the cell colonization and the ECM deposition.

The firm bonding of the coating to the substrate is crucial for the long-term normal function of the bone implants, because the debris exfoliated from the coating can cause aseptic implant loosening and thus failure. The adhesion strength of the coatings to the substrate after immersion in α-MEM for different durations in the absence of cells is shown in Fig. 3c. The Lc values of TCP, C2-TCP, C7-TCP, and C13-TCP without immersion are about 29.5 N in average with no significant difference among the different coatings, indicating a strong and firm bonding of the coatings to the substrates which is not influenced by the Co incorporation. After immersion in α-MEM for as long as 4 weeks, their adhesion

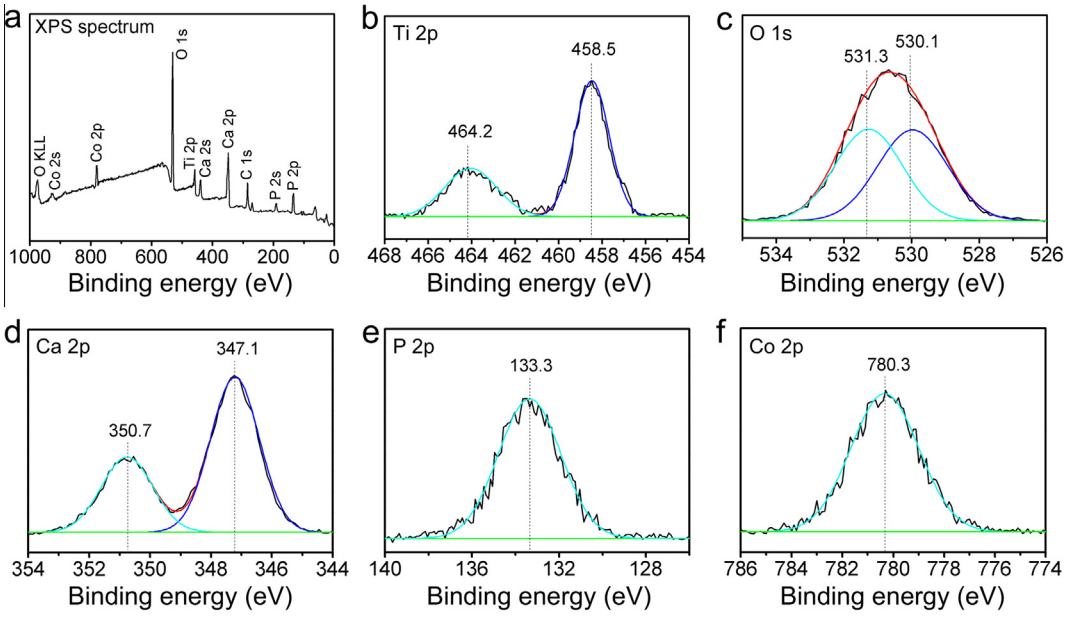

Fig. 2. (a) XPS survey spectrum, and (b) Ti2p, (c) O1s, (d) Ca2p, (e) P2p, and (f) Co2p high-resolution spectra of C7-TCP.

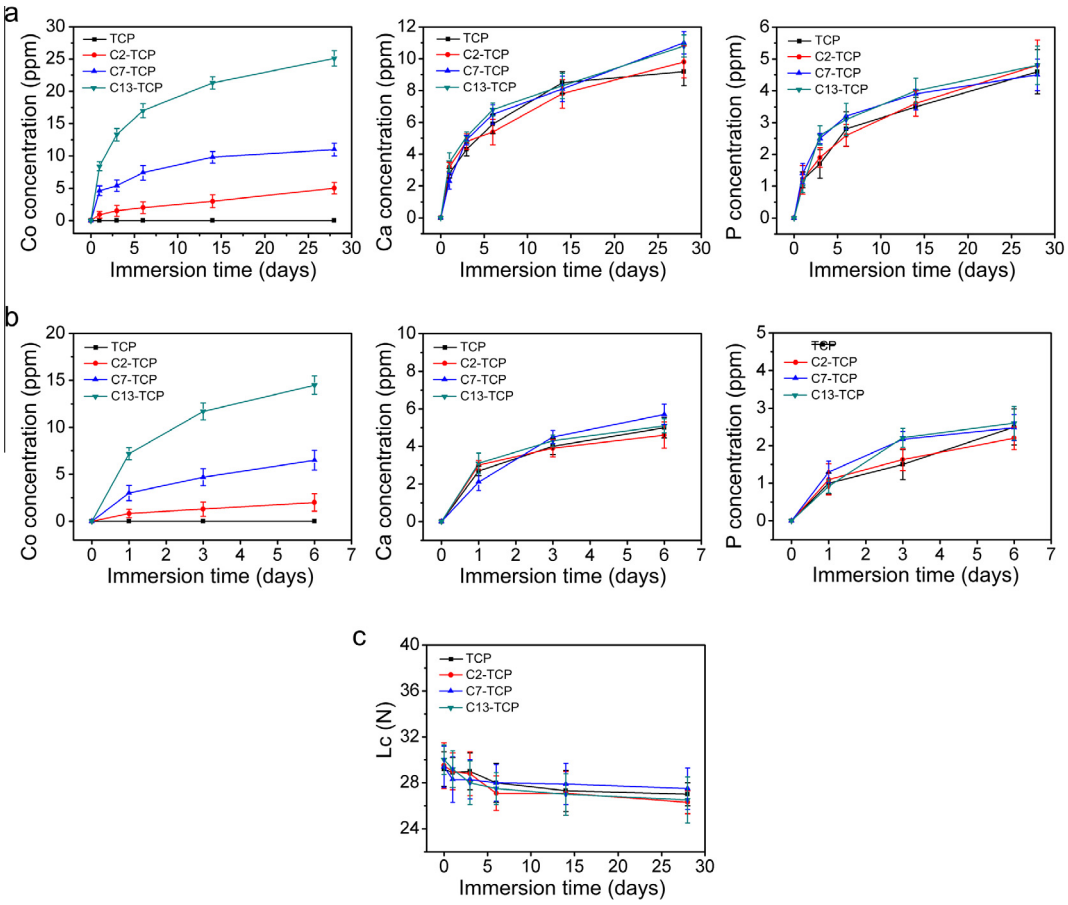

Fig. 3. Cumulative release of Co, Ca, and P of the coatings before and after immersion in α-MEM of different durations in the absence of cells (a) and in the presence of cells (b), and (c) adhesion strength of the coatings before and after immersion in α-MEM without cells.

strength retain well with slight decrease, suggesting the good long-term adhesion strength stability of all the coatings during usage in the biological environment.

The Co incorporation was previously tried on several kinds of biomaterials including bioactive glass, β-tricalcium phosphate ceramics, and hydroxyapatite [17–21]. However, to the best of our knowledge, there has been yet no report on the Co incorporation to the biomedical metal implants and our present study shall provide the first evidence to support the feasibility of fabricating the Co incorporated biomedical metal implant coating. The Co incorporation does not change the microporous structure, the TiO_2 phase composition, the surface roughness or the surface wettability of the microporous TiO_2 coating. The Co containing coating can release the Co ions to induce potential biological effects. Meanwhile, the Co containing coatings bond firmly to the Ti substrate and show good long-term adhesion strength stability accompanied with the Co release in biological environment.

3.3. Protein adsorption, cytotoxicity, cell adhesion, and proliferation

The proteins adsorbed to a biomaterial surface play a pivotal role in conveying the biological effect of the surface topographical cue to the cells/tissues [34]. Hence, the amount of total protein adsorbed onto the coatings from the cell culture medium after 24 h of incubation is measured (Fig. 4a). In comparison with the pristine Ti control, TCP, C2-TCP, C7-TCP, and C13-TCP adsorb more proteins, which can be attributed to their rougher surface with larger surface area. TCP, C2-TCP, C7-TCP, and C13-TCP do not induce obvious difference in the protein adsorption amount, indicating that the Co incorporation has no obvious effect on the protein adsorption amount.

Since Co overdose may lead to cytotoxicity [17], the LDH released by the cells cultured on the Ti samples is evaluated as an index of cytotoxicity. As shown in Fig. 4b, TCP, C2-TCP, and C7-TCP exhibit no cytotoxicity as indicated by the similar LDH release amounts to that of the Ti control. The LDH release amount induced by C13-TCP is slightly higher than that induced by the Ti control, indicating that Co incorporation of 13% into the MAO coating can induce certain cytotoxicity, which is further supported by the subsequent *in vitro* cell adhesion and proliferation results.

Initial cell adhesion is the key step for the ensuing cell functions on biomaterials including proliferation and differentiation [33]. As shown in Fig. 4c, TCP, C2-TCP, C7-TCP, and C13-TCP lead to more initial adherent cells in comparison with the pristine Ti control, in accordance with their larger surface area and more protein adsorption. No obvious difference in the initial adherent cell number is observed among themselves, indicating that the Co incorporation or not as well as the amount of the incorporated Co in the context of present study have a negligible effect on the initial adherent cell number. The ensuing event, cell proliferation, is assessed by CCK-8 (Fig. 4d) and the live/dead staining images are displayed in Fig. 4e. Generally, MSCs proliferate on all the Ti surfaces with time, while difference in cell proliferation is observed among the different Ti surfaces. At all the three time durations concerned here, the cell proliferation on TCP, C2-TCP, and C7-TCP is obviously better than that on the Ti control and no significant difference is found among TCP, C2-TCP, and

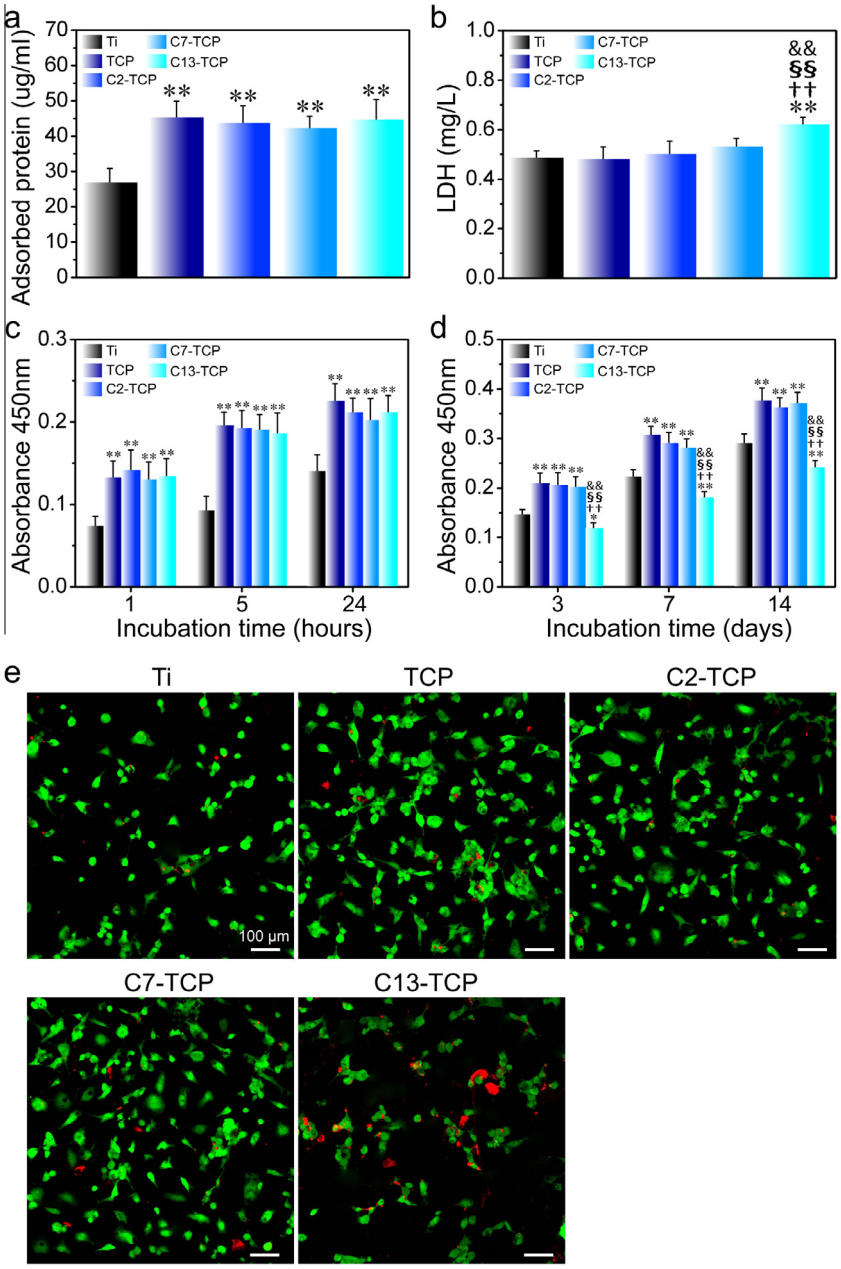

Fig. 4. (a) Protein adsorption to the samples after 24 h of immersion in a-MEM containing 10% FBS, (b) LDH amount released by the cells during the first 3 days of incubation, (c) cell adhesion measured by CCK-8 after 1, 5, and 24 h of culture, (d) cell proliferation measured by CCK-8 after 3, 7, and 14 days of culture, (e) live (green)/dead (red) staining of the cells incubated for 7 days on the samples. Data are presented as mean ± SD, n = 5. $^{**}p < 0.01$ compared to Ti; $^{\dagger\dagger}p < 0.01$ compared to TCP; $^{\S\S}p < 0.01$ compared to C2-TCP; $^{\&\&}p < 0.01$ compared to C7-TCP. (For interpretation of the references to colour in this figure legend, the reader is referred to the web version of this article.)

C7-TCP. In contrast, the cell proliferation on C13-TCP is significantly lower than that on the Ti control, which shall be attributed to the cytotoxicity of C13-TCP. As shown in Fig. 4e, after culturing for 7 days there are sporadic dead cells (red) on Ti, TCP, C2-TCP, and C7-TCP, while the number of dead cells on C13-TCP is obviously larger.

Previous study showed that the Co ions of too high concentrations might cause cytotoxicity [17], and actually it shall be true for all the inorganic bioactive elements. In present study, the concentrations of Co ions released from C2-TCP and C7-TCP are in a relatively low range of no more than 10 ppm, while that from C13-TCP is more than 15 ppm, a relatively high concentration. This can explain theexistence of cytotoxicity for C13-TCP while the not obvious one for C2-TCP and C7-TCP.

3.4. Cell morphology

The cell shape that MSCs assume on a biomaterial surface is affected by the biomaterial surface properties and closely related to the functions and fate of MSCs [35]. Accordingly, the adhesion and spreading of MSCs cultured on the different Ti surfaces are inspected by the FESEM after 3 days of culture (Fig. 5a). MSCs on the flat Ti control spread poorly with a spindle shape indicative of undifferentiated quiescent cells. Whereas, TCP, C2-TCP, C7-TCP, and C13-TCP greatly improve the attachment and spreading of MSCs. On them, the cell bodies of MSCs either cover or anchor to the micropores on the Ti surfaces, as indicated by the red arrows in Fig. 5a, which may be the reason that the ion release of coating in the presence of cells is lower than that

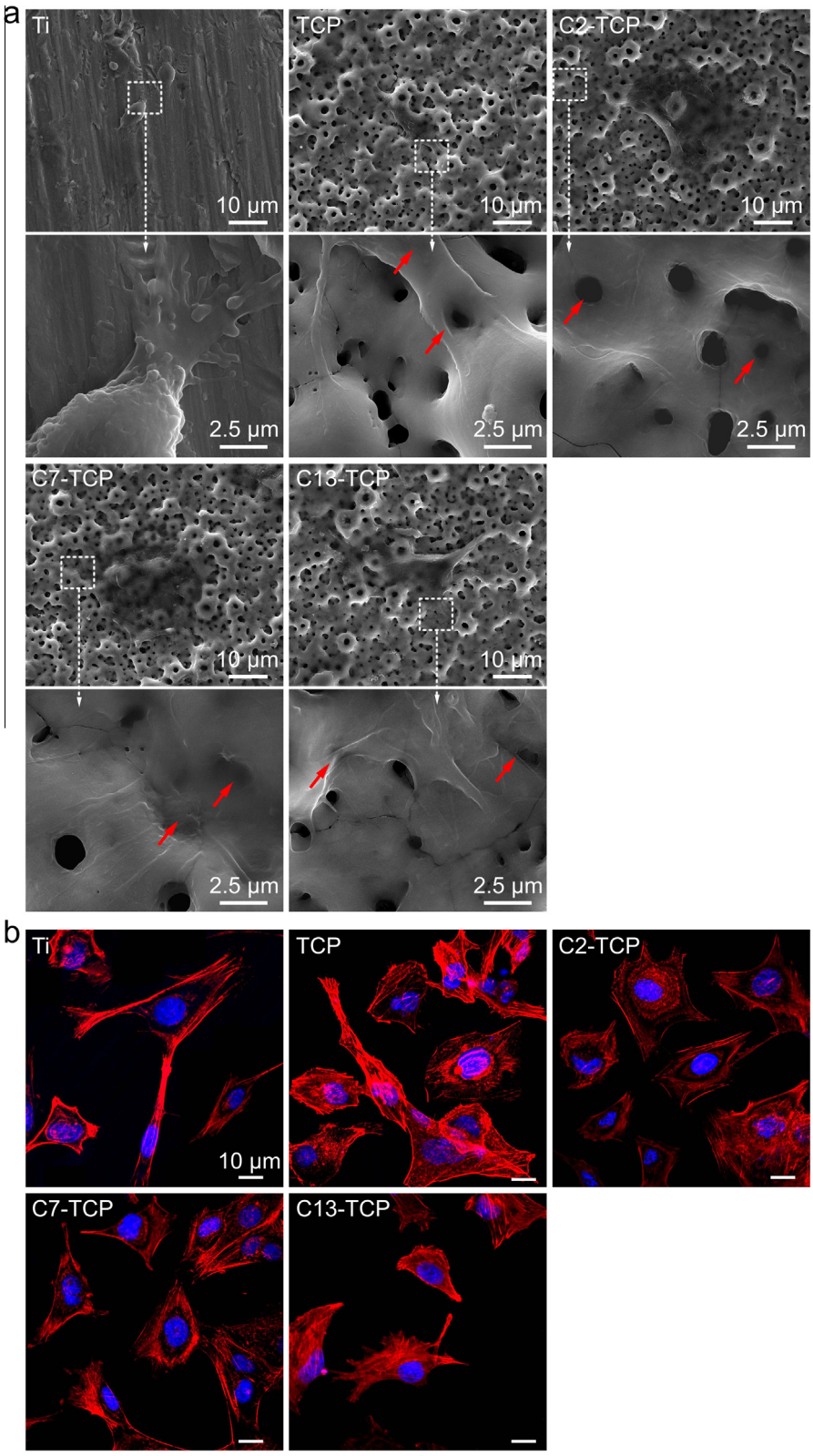

Fig. 5. (a) SEM observation and (b) actin (red) and nucleus (blue) fluorescence images of MSCs after 3 days of culture on the different Ti samples. (For interpretation of the references to colour in this figure legend, the reader is referred to the web version of this article.)

in the absence of cells. MSCs assume a well extended flat polygonal shape and attach intimately to the substrate well along the micro-texture. The higher magnification images display that there were no obvious filopodia on flat Ti. On contrary, TCP, C2-TCP, C7-TCP, and C13-TCP induce many filopodia attaching closely to the coatings. Similar trend in cell spreading area has been found via the confocal laser scanning microscopy after 3 days of culture (Fig. 5b).

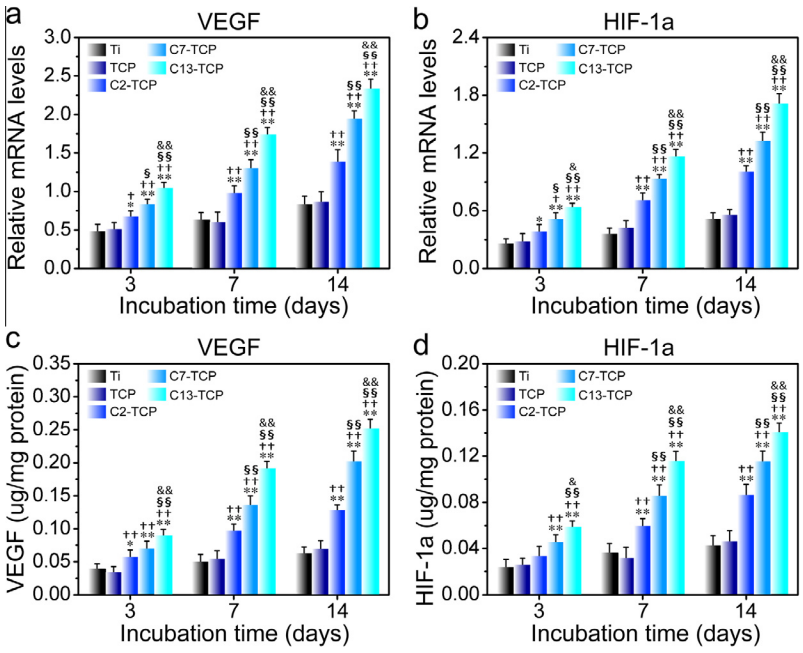

Fig. 6. (a) Gene expression and (b) intracellular protein product of VEGF and HIF-1a in MSCs cultured on the coatings for 3, 7, and 14 days. The gene expression values are normalized to GAPDH. Data are presented as mean ± SD, n = 5. $^{*}p < 0.05$ and $^{**}p < 0.01$ compared to Ti; $^{\dagger}p < 0.05$ and $^{\dagger\dagger}p < 0.01$ compared to TCP; $^{\S}p < 0.05$ and $^{\S\S}p < 0.01$ compared to C2-TCP; $^{\&}p < 0.05$ and $^{\&\&}p < 0.01$ compared to C7-TCP.

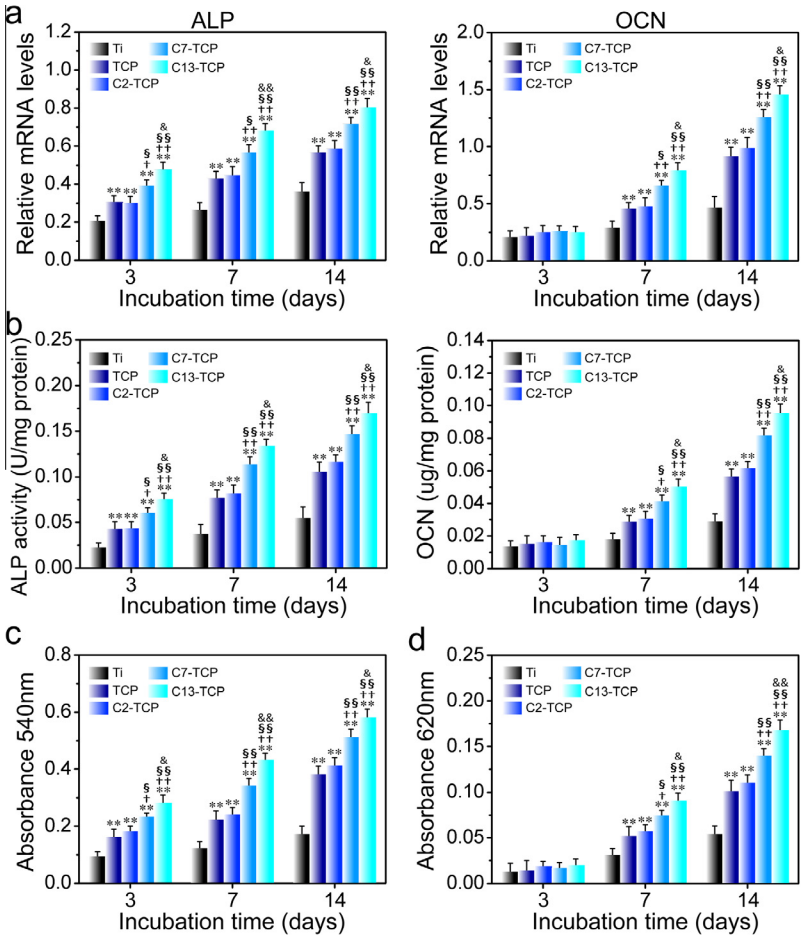

Fig. 7. (a) Gene expression of ALP and OCN, (b) intracellular ALP activity and OCN protein product, (c) collagen secretion, and (d) ECM mineralization after 3, 7, and 14 days incubation of MSCs on the coatings. The gene expression values are normalized to GAPDH. Data are presented as mean ± SD, n = 5. $^{*}p < 0.05$ and $^{**}p < 0.01$ compared to Ti; $^{\dagger}p < 0.05$ and $^{\dagger\dagger}p < 0.01$ compared to TCP; $^{\S}p < 0.05$ and $^{\S\S}p < 0.01$ compared to C2-TCP; $^{\&}p < 0.05$ and $^{\&\&}p < 0.01$ compared to C7-TCP.

3.5. Angiogenic activity

After culturing on the Ti samples for 3, 7, and 14 days, the gene expression and protein product of key angiogenic factors (VEGF and HIF-1a) in MSCs are measured using the Quantitative real-time PCR and ELISA assays, respectively (Fig. 6). It can be seen that the VEGF and HIF-1a gene expression and protein product in MSCs on the Ti surfaces followed the rank of C13-TCP > C7-TCP > C2-TCP > TCP ≈ Ti, indicating that the Co incorporation remarkably increases the expression of the angiogenic factors positively related to the incorporated Co amount. Meanwhile, the similar expression of the angiogenic factors between TCP and Ti suggest that the MAO microporous structure with Ca/P has no obvious angiogenesis improving activity.

Numerous studies have revealed that Co can significantly stimulate new vessel formation [17–21]. A widely accepted mechanism is that it can mimic the hypoxia condition via stabilizing HIF-1a to activate the VEGF expression that is associated with neovascularization and tissue regeneration [15,16]. The data from the bioactive glass, β-tricalcium phosphate ceramics, and hydroxyapatite showed that the Co incorporation and release could surely mimic a hypoxia condition and thus improve the angiogenic property of biomaterials by up-regulating the HIF-1a and VEGF expression [17–21]. Our data on the biomedical metal implant that the Co-incorporated coatings enhance the gene expression and protein synthesis of HIF-1a and VEGF in MSCs provide more evidence to support the angiogenic ability of Co as well as the versatility of the Co incorporation and delivery to improve the angiogenic activity of biomaterials.

3.6. Osteogenic activity

Quantitative real-time PCR assay is performed to detect the gene expression of osteogenic factors (ALP and OCN) in MSCs after culturing on various Ti samples for 3, 7, and 14 days. Meanwhile, the intracellular ALP activity, OCN protein product, collagen secretion and ECM mineralization are also measured (Fig. 7). Totally, the expression of all the surrogate osteogenesis related markers follows the rank of C13-TCP > C7-TCP > C2-TCP ≈ TCP > Ti. The data demonstrate that the microporous coatings with Co incorporation or not possess the osteogenesis improving effect compared to the flat Ti control. In addition, C13-TCP and C7-TCP induce significantly enhanced expression of osteogenesis related markers compared to TCP and C2-TCP, while TCP and C2-TCP have similar expression. Hence, the Co incorporation can show osteogenesis improving effect. The effect is positively related to the Co incorporation dose with a threshold.

Except inducing angiogenesis, there were reports indicating that Co also displayed the osteogenesis stimulating effect [17–19]. Our data are in line with these previous reports. The osteogenesis improving efficacy for the Co incorporation is closely related to the Co amounts with >7%% of incorporated Co significantly enhancing the osteogenic activity.

4. Conclusion

The microporous TiO_2/Ca-P coating doped with Co of tunable amount has been successfully developed through a simple MAO procedure. The microstructure, TiO_2 phase compositions, surface roughness, wettability of the TiO_2/Ca-P coating are not apparently affected by the Co incorporation. The Co containing coatings bond firmly to the Ti substrate and show good long-term adhesin strength stability with the Co release in the biological environment. The Co incorporation leads to improvement in both angiogenesis and osteogenesis, and the effects are positively related to the incorporated Co amount. Overdose of Co incorporation (C13-TCP) can induce certain cytotoxicity. In the context of present study, C7-TCP gives rise to the best performance, inducing obviously promoted angiogenic and osteogenic activities with no significant cytotoxicity and thus being highly promising to achieve advanced implants of both angiogenic and osteogenic activities.

Competing financial interests

The authors declare no competing financial interest.

Acknowledgements

We appreciate the National Natural Science Foundation of China (81401527 and 31570954), China Postdoctoral Science Foundation (2014M560771 and 2016T90912), Postdoctoral Research Program of Shaanxi Province, National High Technology Research and Development Program of China (SS2015AA020921), A Foundation for the Author of National Excellent Doctoral Dissertation of PR China (FANEDD, No. 201483), Natural Science Foundation of Shaanxi Province (2015JM8387), and Baoji University of Arts and Sciences Key Research (ZK15042) for financially supporting this work.

References

[1] T. Albrektsson, P.I. Brånemark, H.A. Hansson, J. Lindström, Osseointegrated titanium implants. Requirements for ensuring a long-lasting, direct bone-to-implant anchorage in man, Acta Orthop. Scand. 52 (1981) 155–170.
[2] D.F. Williams, Titanium and titanium implants, in: D.F. Williams (Ed.), Biocompatibility of Clinical Implant Materials, CRC Press, vol. 1, Boca Raton, Florida, 1981, pp. 9–44.
[3] I.D. Learmonth, C. Young, C. Rorabeck, The operation of the century: total hip replacement, Lancet 370 (2007) 1508–1519.
[4] R. Tasso, F. Fais, D. Reverberi, F. Tortelli, R. Cancedda, The recruitment of two consecutive and different waves of host stem/progenitor cells during the development of tissue-engineered bone in a murine model, Biomaterials 31 (2010) 2121–2129.
[5] J.Y. Park, J.E. Davies, Red blood cell and platelet interactions with titanium implant surfaces, Clin. Oral Implants Res. 11 (2000) 530–539.
[6] M. Nomi, A. Atala, P.D. Coppi, S. Soker, Principals of neovascularization for tissue engineering, Mol. Aspects Med. 23 (2002) 463–483.
[7] A. Perets, Y. Baruch, F. Weisbuch, G. Shoshany, G. Neufeld, S. Cohen, Enhancing the vascularization of three-dimensional porous alginate scaffolds by incorporating controlled release basic fibroblast growth factor microspheres, J. Biomed. Mater. Res. A 65 (2003) 489–497.
[8] Y.C. Huang, D. Kaigler, K.G. Rice, P.H. Krebsbach, D.J. Mooney, Combined angiogenic and osteogenic factor delivery enhances bone marrow stromal cell-driven bone regeneration, J. Bone Miner. Res. 20 (2005) 848–857.
[9] D. Kaigler, Z. Wang, K. Horger, D.J. Mooney, P.H. Krebsbach, VEGF scaffolds enhance angiogenesis and bone regeneration in irradiated osseous defects, J. Bone Miner. Res. 21 (2006) 735–744.
[10] E.J. Battegay, J. Rupp, L. Iruela-Arispe, E.H. Sage, M. Pech, PDGF-BB modulates endothelial proliferation and angiogenesis in vitro via PDGF beta-receptors, J. Cell Biol. 125 (1994) 917–928.
[11] F. Liu, X. Zhang, X. Yu, Y. Xu, T. Feng, D. Ren, In vitro study in stimulating the secretion of angiogenic growth factors of strontium-doped calcium polyphosphate for bone tissue engineering, J. Mater. Sci. Mater. Med. 22 (2011) 683–692.
[12] L. Zhao, H. Wang, K. Huo, L. Cui, W. Zhang, H. Ni, Y. Zhang, Z. Wu, P.K. Chu, Antibacterial nano-structured titania coating incorporated with silver nanoparticles, Biomaterials 32 (2011) 5706–5716.
[13] M. Kobayashi, S. Shimizu, Cobalt proteins, Eur. J. Biochem. 261 (1999) 1–9.
[14] C.G. Fraga, Relevance, essentiality and toxicity of trace elements in human health, Mol. Aspects Med. 26 (2005) 235–244.
[15] H.H. Kim, S.E. Lee, W.J. Chung, Y. Choi, K. Kwack, S.W. Kim, H. Park, Z.H. Lee, Stabilization of hypoxia-inducible factor-1alpha is involved in the hypoxic stimuli-induced expression of vascular endothelial growth factor in osteoblastic cells, Cytokine 17 (2002) 14–27.
[16] E. Pacary, H. Legros, S. Valable, P. Duchatelle, M. Lecocq, E. Petit, O. Nicole, M. Bernaudin, Synergistic effects of CoCl(2) and ROCK inhibition on mesenchymal stem cell differentiation into neuron-like cells, J. Cell Sci. 119 (2006) 2667–2678.
[17] C. Wu, Y. Zhou, W. Fan, P. Han, J. Chang, J. Yuen, M. Zhang, Y. Xiao, Hypoxia-mimicking mesoporous bioactive glass scaffolds with controllable cobalt ion release for bone tissue engineering, Biomaterials 33 (2012) 2076–2085.

[18] Z. Chen, J. Yuen, R. Crawford, J. Chang, C. Wu, Y. Xiao, The effect of osteoimmunomodulation on the osteogenic effects of cobalt incorporated β-tricalcium phosphate, Biomaterials 61 (2015) 126–138.
[19] E. Quinlan, S. Partap, M.M. Azevedo, G. Jell, M.M. Stevens, F.J. O'Brien, Hypoxia-mimicking bioactive glass/collagen glycosaminoglycan composite scaffolds to enhance angiogenesis and bone repair, Biomaterials 52 (2015) 358–366.
[20] K. Senthilguru, M. Upasana, A. Tarun, G. Supratim, P. Kunal, P. Krishna, B. Indranil, Improving the osteogenic and angiogenic properties of synthetic hydroxyapatite by dual doping of bivalent cobalt and magnesium ion, Ceram. Int. 41 (2015) 11323–11333.
[21] M. Zhang, C. Wu, H. Li, J. Yuen, J. Chang, Y. Xiao, Preparation, characterization and in vitro angiogenic capacity of cobalt substituted b-tricalcium phosphate ceramics, J. Mater. Chem. 22 (2012) 21686–21694.
[22] D. Wei, Y. Zhou, D. Jia, Y. Wang, Characteristic and in vitro bioactivity of a microarc-oxidized TiO(2)-based coating after chemical treatment, Acta Biomater. 3 (2007) 817–827.
[23] Y. Han, D.H. Chen, L. Zhang, Nanocrystallized SrHA/SrHA-$SrTiO_3$/$SrTiO_3$-TiO_2 multilayer coatings formed by micro-arc oxidation for photocatalytic application, Nanotechnology 19 (2008) 335705–335712.
[24] W. Liu, M. Cheng, T. Wahafu, Y. Zhao, H. Qin, J. Wang, X. Zhang, L. Wang, The in vitro and in vivo performance of a strontium-containing coating on the low-modulus Ti35Nb2Ta3Zr alloy formed by micro-arc oxidation, J. Mater. Sci. Mater. Med. 26 (2015) 203–216.
[25] H. Hu, W. Zhang, Y. Qiao, X. Jiang, X. Liu, C. Ding, Antibacterial activity and increased bone marrow stem cell functions of Zn-incorporated TiO_2 coatings on titanium, Acta Biomater. 8 (2012) 904–915.
[26] D. Sakai, J. Mochida, Y. Yamamoto, T. Nomura, M. Okuma, K. Nishimura, T. Nakai, K. Ando, T. Hotta, Transplantation of mesenchymal stem cells embedded in Atelocollagens gel to the intervertebral disc:a potential therapeutic model for disc degeneration, Biomaterials 24 (2003) 3531–3541.
[27] C. Viornery, Y. Chevolot, D. Léonard, B.O. Aronsson, P. Péchy, H.J. Mathieu, P. Descouts, M. Grätzel, Surface modification of titanium with phosphonic acid to improve bone bonding: characterization by XPS and ToF-SIMS, Langmuir 18 (2002) 2582–2589.
[28] Y. Han, D. Chen, J. Sun, Y. Zhang, UV-enhanced bioactivity and cell response of micro-arc oxidized titania coatings, Acta Biomater. 4 (2008) 1518–1529.
[29] Z.Q. Yao, Y. Ivanisenko, T. Diemant, A. Caron, A. Chuvilin, J.Z. Jiang, R.Z. Valiev, M. Qi, H.J. Fecht, Synthesis and properties of hydroxyapatite-containing porous titania coating on ultrafine-grained titanium by micro-arc oxidation, Acta Biomater. 6 (2010) 2816–2825.
[30] A. Dupraz, T.P. Nguyen, M. Richard, G. Daculsi, N. Passuti, Influence of a cellulosic ether carrier on the structure of biphasic calcium phosphate ceramic particles in an injectable composite material, Biomaterials 20 (1999) 663–673.
[31] C.C. Chusuei, D.W. Goodman, M.J. Van Stipdonk, D.R. Justes, E.A. Schweikert, Calcium phosphate phase identification using XPS and time-of-flight cluster SIMS, Anal. Chem. 71 (1999) 149–153.
[32] B. Sarkar, C. Pendem, L.N. Sivakumar Konathala, T. Sasaki, R. Bal, Formation of ilmenite-type $CoTiO_3$ on TiO_2 and its performance in oxidative dehydrogenation of cyclohexane with molecular oxygen, Catal. Commun. 56 (2014) 5–10.
[33] K. Anselme, Osteoblast adhesion on biomaterials, Biomaterials 2 (2000) 667–681.
[34] M.S. Lord, M. Foss, F. Besenbacher, Influence of nanoscale surface topography on protein adsorption and cellular response, Nano Today 5 (2010) 66–78.
[35] R. McBeath, D.M. Pirone, C.M. Nelson, K. Bhadriraju, C.S. Chen, Cell shape, cytoskeletal tension, and RhoA regulate stem cell lineage commitment, Dev. Cell 6 (2004) 483–495.